RSC Advances

PAPER

View Article Online
View Journal | View Issue



Cite this: *RSC Adv.*, 2017, **7**, 24177

# Effect of the calcination temperature of cerium–zirconium mixed oxides on the structure and catalytic performance of $WO_3/CeZrO_2$ monolithic catalyst for selective catalytic reduction of $NO_x$ with $NH_3$

Haidi Xu,[a] Mengmeng Sun,[a] Shuang Liu,[b] Yuanshan Li,[c] Jianli Wang*[b] and Yaoqiang Chen *[abc]

A series of $WO_3/CeZrO_2$ catalysts, prepared at different calcination temperatures (400, 500, 600 and 700 °C) of cerium–zirconium mixed oxides ($CeZrO_2$) for the selective catalytic reduction of $NO_x$ with ammonia ($NH_3$-SCR), were investigated *via* various characterizations, such as $N_2$ physisorption, XRD, Raman, $NH_3$-TPD, DRIFTS, XPS and $H_2$-TPR. The catalytic performance of $NH_3$-SCR was remarkably promoted by modestly increasing the calcination temperature of $CeZrO_2$: $WO_3/CeZrO_2$-500 possessed the lowest light-off temperature (173 °C) and complete conversion temperature (205 °C), while W/$CeZrO_2$-600 could achieve greater than 90% $NO_x$ conversion in a broad temperature range of 220–455 °C. The characterization results indicated that modest enhancement of the calcination temperature of $CeZrO_2$ was beneficial to stabilizing the structure of the catalysts. The largest amount of Lewis acid sites, $Ce^{3+}$ and surface active oxygen species, as well as strong redox properties of $WO_3/CeZrO_2$-500 should together contribute to its better low-temperature de$NO_x$ activity. Moreover, increasing the calcination temperature of cerium–zirconium mixed oxides resulted in the enhancement of Brønsted acid sites, which was responsible for the widened operation temperature window. Therefore, $WO_3/CeZrO_2$ serial catalysts with appropriate calcination treatment of $CeZrO_2$ would be a good choice for the removal of $NO_x$ emitted from diesel engines.

Received 14th March 2017
Accepted 18th April 2017

DOI: 10.1039/c7ra03054a

rsc.li/rsc-advances



## 1 Introduction

Nitrogen oxides ($NO_x$), caused by fossil fuel combustion, are notable and known as the major causes of haze, photochemical smog, acid rain, ozone depletion and the greenhouse effect, among various air contaminants. The technique of selective catalytic reduction of $NO_x$ with $NH_3$ ($NH_3$-SCR) is the most widely and efficiently employed to control $NO_x$ emitted from the coal-fired power plants and the diesel engines, and $V_2O_5$–$WO_3/TiO_2$ is currently the most commercially used $NH_3$-SCR catalyst in the industry.[1–3] However, some disadvantages still exist in this catalyst system, such as poor thermal stability, narrow operating temperature window, the unselective oxidation of $NH_3$, which produces the ozone-depleting, greenhouse gas, $N_2O$, at high temperatures, and sublimated $V_2O_5$ generates biological toxicity in the environment.[2,4] In order to overcome the above problems and meet the EURO VI standard, it is greatly significant to develop novel eco-friendly $NH_3$-SCR catalysts with outstanding low-temperature de$NO_x$ conversion, wide operation temperature window and high $N_2$ selectivity.

Recently, $CeO_2$ has been extensively used in various catalytic reactions due to its being non-toxic, inexpensive and having oxygen storage/release properties. Moreover, the addition of $ZrO_2$ into $CeO_2$ can obviously promote the thermal stability and oxygen storage properties of pure $CeO_2$.[5,6] In fact, cerium–zirconium mixed oxides have been demonstrated to be one of the most promising materials for de$NO_x$ among the new vanadium-free catalytic systems. Li *et al.*[7] reported that the $WO_3/CeO_2$–$ZrO_2$ catalyst was efficient for $NH_3$-SCR and 10 wt% $WO_3/CeO_2$–$ZrO_2$ could achieve nearly 100% $NO_x$ conversion in the temperature range of 200–500 °C with 1 : 1 (molar ratio) of $NO/NO_2$; furthermore, it displayed higher thermal stability than the conventional $V_2O_5$–$WO_3/TiO_2$ catalyst under similar reaction conditions.

Cerium–zirconium mixed oxides have recently attracted significant attention and have been modified to improve their catalytic performance in the field of $NH_3$-SCR. Si *et al.*[8] found

[a]*Institution of New Energy and Low-Carbon Technology, Sichuan University, Chengdu, 610064, PR China . E-mail: nic7501@scu.edu.cn; Fax: +86-28-85418451; Tel: +86-28-85418451*

[b]*College of Chemistry, Sichuan University, Chengdu 610064, PR China. E-mail: wangjianli@scu.edu.cn; Fax: +86-28-85418451; Tel: +86-28-85418451*

[c]*College of Chemical Engineering, Sichuan University, Chengdu 610064, PR China*

that more than 80% $NO_x$ could be converted over 3.8% NiO-6.2% $SO_4^{2-}/CeO_2$–$ZrO_2$ catalyst in the temperature range of 280–400 °C, which could result from the fact that the addition of Ni improved the Lewis acidity of $CeO_2$–$ZrO_2$ to increase the low-temperature activity, and Brønsted acid sites introduced by $SO_4^{2-}$ facilitated $NH_3$ adsorption instead of $NH_3$ oxidation to promote the high-temperature activity. $NbO_x$ supported on $Ce_{0.75}Zr_{0.25}O_2$ can also effectively enhance the de$NO_x$ activity of cerium–zirconium mixed oxides for the increase of active sites and surface acidity.[9] In addition, Ding *et al.*[1] believed that the introduction of Nb remarkably improved the $SO_2/H_2O$ resistance and hydrothermal ability of $CeZrO_x$. Zhang and his group reported that the $NH_3$-SCR performance of $MnO_x/CeO_2$–$ZrO_2$ was significantly dependent on the morphology of $Ce_{0.9}Zr_{0.1}O_2$; the catalyst nanorods having more $Mn^{4+}$ and adsorbed surface oxygen as well as oxygen vacancies displayed higher $NO_x$ conversion than nanotubes and nanopolyhedra.[10,11] Our previous works showed that the Fe–W/$Ce_{0.68}Zr_{0.32}O_2$ with Ce/Zr (molar ratio) of 68 : 32 displayed the best $NH_3$-SCR performance, compared to other Fe–W/$Ce_xZr_{1-x}O_2$ with different Ce/Zr.[12,13] In the above studies, it has been found that the $NH_3$-SCR activity of $WO_3/CeZrO_2$ catalyst was obviously affected by the calcination temperature of the carrier; however, the optimum calcination temperature of cerium–zirconium mixed oxides and the effects of the calcination temperature on the $NH_3$-SCR performance of catalysts have not been investigated to our knowledge, which should play a key role in the practical application of the serial catalysts.

In the present study, a series of $WO_3/CeZrO_2$ catalysts with different calcination temperatures of $CeZrO_2$ were employed for the $NH_3$-SCR reaction, and the optimum calcination temperature of the carrier and its effects on the $NH_3$-SCR performance were studied separately. The relationships among catalytic activity, structure and surface acidy sites are explored herein. $N_2$ physisorption, XRD, Raman, $H_2$-TPR, XPS, $NH_3$-TPD and $NH_3$-DRIFTS were employed to characterize the physical and chemical properties of the catalysts.

# 2. Experimental

## 2.1 Catalyst preparation

The carrier material, cerium–zirconium mixed oxides ($CeZrO_2$, denoted as CZ), was prepared by the conventional co-precipitation method with $CeO_2/ZrO_2$ = 68/32 molar ratio; the detailed preparation process has been described in our previous study.[13] The obtained precipitate was filtered and washed by deionized water, followed by dried at 70 °C for 24 h and at 400, 500, 600 and 700 °C for 3 h, respectively. Finally, CZ-*T* (where *T* is the calcination temperature, *e.g.* 400 °C) powders were obtained as carriers. A series of W/CZ-*T* catalysts with 10 wt% $WO_3$ were prepared by supporting the precursor ammonium metatungstate (AR grade, 99%, Anda, China) on CZ-*T* using the incipient wetness impregnation method. The obtained catalyst powders were dried at 70 °C for 24 h, and then calcined at 500 °C for 3 h in air (except that the W/CZ-400 catalyst was calcined at 400 °C). The resulting four catalyst powders were subsequently coated on honeycomb cordierites (cylinder, diameter: 11 mm, length: 26 mm, bulk: 2.5 $cm^3$, 62 cell per $cm^2$, Corning, USA), and then dried at 120 °C overnight and calcined at 400 °C (only the W/CZ-400 catalyst) or 500 °C for 3 h. Finally, a series of W/CZ-*T* monolithic catalysts with the coating content of about 160 g $L^{-1}$ was obtained.

## 2.2 Catalytic activity measurements

The $NH_3$-SCR activity measurements of the prepared monolithic catalysts were carried out in a fixed-bed quartz tube flow reactor at atmospheric pressure. The flue gas composition was as follows: 500 ppm NO, 500 ppm $NH_3$, 5% $O_2$, balance $N_2$. The premixed gases (2.0% NO in $N_2$, 2.0% $NH_3$ in $N_2$ and 99.99% $O_2$) were supplied by Testing Technology Research Institute, China. Reactant gases were regulated by mass-flow controllers before entering the reactor. Under typical conditions, 2.5 $cm^3$ monolithic catalyst sample was used in each run and the total flow rate was about 1250 mL $min^{-1}$, yielding the GHSV of 30 000 $h^{-1}$ by volume. The separate $NH_3$/NO oxidation activity was tested in the absence of NO/$NH_3$, respectively. The concentrations of $NH_3$, $NO_x$ and $N_2O$ in the inlet and outlet gases were continually analyzed by an FT-IR (Antaris IGS, Nicolet). The data were recorded after 30 min when the reaction reached a steady state for each test.

The $NO_x/NH_3$ conversions ($X_{NO_x}/X_{NH_3}$) and $N_2$ selectivity ($S_{N_2}$) were calculated as follows:

$$X_{NO_x}/X_{NH_3}\ (\%) = \frac{C_{in} - C_{out}}{C_{in}} \times 100 \quad (1)$$

$$S_{N_2}\ (\%) = \left(1 - \frac{2[N_2O]_{out}}{([NO_x]_{in} - [NO_x]_{out}) + ([NH_3]_{in} - [NH_3])_{out}}\right) \times 100 \quad (2)$$

where, $[NO_x] = [NO] + [NO_2]$, $C_{in}$ and $C_{out}$ denote the inlet and outlet gas concentrations of $NO_x$ or $NH_3$, respectively.

## 2.3 Characterizations

The textural properties of all catalysts were measured by $N_2$ adsorption–desorption at −196 °C on a Quantachrome automated surface area & pore size analyzer (Autosorb SI). The samples were pretreated at 300 °C for 3 h prior to the measurement. The surface areas were determined by the Brunauer–Emmett–Teller (BET) model.

Powder X-ray diffraction (XRD) patterns of samples were collected in the 2$\theta$ range of 10–80° using a Rigaku D/max-RA diffractometer equipped with a Cu $K_\alpha$ ($\lambda$ = 0.15406 nm) radiation resource operated at 40 kV and 100 mA, respectively.

Visible Raman spectra of all catalysts were collected on a Lab-RAM HR laser Raman spectrograph with a spectral resolution of 2 $cm^{-1}$ at room temperature. A Nd:Yag laser of 532 nm was used as the excitation source, with a power output of 30 mW. All specimens were illuminated through a 50× objective and in powder form to prevent diffusion problems. Raman spectra were collected and recorded over the spectral range of

 

200–1000 $cm^{-1}$. The specification of the grating was 600 g $mm^{-1}$.

The *in situ* diffuse-reflectance infrared Fourier transform spectroscopy (DRIFTS) of adsorbed species arising from $NH_3$ adsorption at various temperatures over the catalysts, were collected in the range of 4000–650 $cm^{-1}$ using Thermo Nicolet 6700 FTIR spectrometer. Diffuse reflectance measurements were performed *in situ* in a high temperature cell equipped with a KBr window. The catalyst was heated to 350 °C under $N_2$ at a total flow rate of 100 mL $min^{-1}$ for 1 h to remove any adsorbed impurities, then it was cooled down to 50 °C, exposed to 1000 ppm $NH_3/N_2$ (100 mL $min^{-1}$) for 1 h, and subsequently flushed with $N_2$. Afterwards, the DRIFTS spectra of catalysts were collected between 50 and 300 °C at a 50 °C interval. The background spectrum was collected once every 50 °C in the flowing $N_2$ during the cooling process.

$NH_3$-TPD experiments were carried out in a fixed-bed quartz reactor. A typical sample mass of 100 mg and a gas flow rate of 30 mL $min^{-1}$ were used during the experiments. The experiment included four stages: (1) degasification of the sample in $N_2$ at 400 °C for 1 h to clear the surface, (2) adsorption of 2 vol% $NH_3$-98% $N_2$ at 120 °C for 1 h, (3) isothermal desorption in $N_2$ at 120 °C until no $NH_3$ was detected and (4) temperature programmed desorption in $N_2$ at 10 °C $min^{-1}$ up to 500 °C. The detector was a thermal conductivity detector.

The X-ray photoelectron spectral (XPS) data were recorded on a Thermo Escalab 250Xi electron spectrophotometer at 15 kV and 14.9 mA electric current using Al $K_\alpha$ radiation (1486.6 eV), and operating in a constant pass energy mode (20 eV pass energy). The C 1s peak at 284.8 eV was used for the calibration of binding energy values, and the semi-quantitative surface relative atomic concentrations were obtained from eqn (3). The pressure in the analytical chamber was about $10^{-8}$ Pa.

$$\frac{n_i}{n_j} = \frac{I_i}{I_j} \times \frac{\sigma_j}{\sigma_i} \times \frac{E_{kj}^{0.5}}{E_{ki}^{0.5}} \quad (3)$$

where $n$ is the surface atomic concentration; $I$ is the intensity or area of the XPS peak; $\sigma$ is the photo-ionization cross-section of the corresponding energy level of the element, using Scofield data; $E_k$ is the kinetic energy of photoelectron, $E_k = h\nu - \text{B.E.}$ (Al K$\alpha$, $h\nu = 1486.6$ eV); i and j are the corresponding elements of the samples.

Temperature programmed reduction of $H_2$ ($H_2$-TPR) experiments were performed in TP-5076 (Xianquan, Tianjin) with a thermal conductivity detector. All catalysts (100 mg) were pretreated in a quartz tubular mico-reactor in a flow of $N_2$ at 450 °C for 1 h to yield a clean surface, and then cooled down to room temperature. The reduction was carried out in a flow of 5 vol% $H_2$ to 95 vol% $N_2$ to 750 °C, with a heating rate of 10 °C $min^{-1}$.

# 3 Results and discussion

## 3.1 Catalytic performance

**3.1.1 $NH_3$-SCR activity.** Fig. 1 displays the catalytic activity of $NH_3$-SCR over W/CZ-*T* catalysts with different calcination temperatures of the carrier. W/CZ-400 showed the poorest $NO_x$ conversion in the whole reaction temperature range: its maximum $NO_x$ conversion was only about 95% at 340 °C and its light-off temperature $T_{50}$ (the temperature at 50% $NO_x$ conversion) was about 212 °C. With the increase of calcination temperature, it could be seen that $NO_x$ conversion was obviously improved and the reaction temperature window (the temperature range of above 90% $NO_x$) was also broadened from Fig. 1a. W/CZ-500 presented the best low-temperature SCR activity, its $T_{50}$ and $T_{90}$ (the temperature at 90% $NO_x$ conversion) were only about 173 and 205 °C, respectively, and higher than 90% $NO_x$ conversion could be achieved in the temperature range of 205–420 °C. Compared with W/CZ-500, the $T_{50}$ and $T_{90}$ of W/CZ-600 slightly shifted to higher temperatures of about 180 and 220 °C, respectively, but its operation temperature window was evidently extended to 220–455 °C. The catalytic activity obviously decreased over W/CZ-700 with $T_{50}$ of 195 °C and $T_{90}$ of 265 °C. In Fig. 1b, the $N_2$ selectivity of all catalysts was nearly 100% in the whole temperature range, except for a slight decline (still above 96%) above 400 °C, which may be due to the non-selective oxidation of $NH_3$ to NO. The $N_2O$ generated concentrations of W/CZ-*T* catalysts in the $NH_3$-SCR reaction were inserted in Fig. 1a, the $N_2O$ concentration was lower than 5 ppm over all catalysts, further indicating that the decrease in the

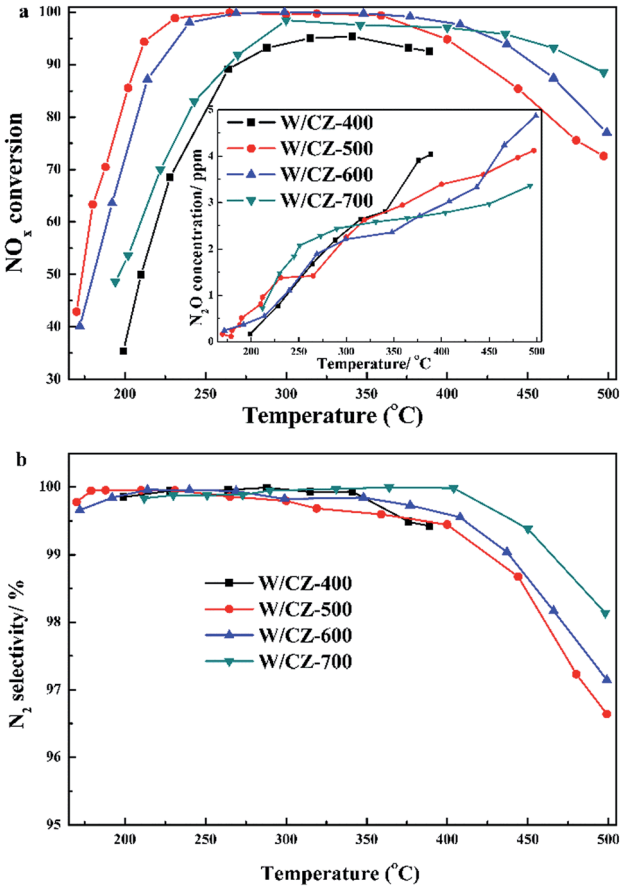


Fig. 1 Effects of calcination temperature of carrier on $NH_3$-SCR performance (a) and $N_2$ selectivity (b) of W/CZ-*T* catalysts. Reaction conditions: 500 ppm NO, 500 ppm $NH_3$, 5% $O_2$, $N_2$ as balance, total flow rate: 1250 mL $min^{-1}$, GHSV: 30 000 $h^{-1}$.

high-temperature $NO_x$ conversion mainly resulted from the non-selective oxidation of $NH_3$ to $NO_x$ for all catalysts. The above results suggest that the calcination temperature obviously affected the $NH_3$-SCR performance of W/CZ catalysts, and the promotional effects were investigated *via* the following characterizations.

**3.1.2 Separated NO/$NH_3$ oxidation.** It is well known that $NO_2$ plays a significant role in the $NH_3$-SCR reaction, especially in the low temperature range; the oxidation of NO to $NO_2$ is very important for promoting the low-temperature de$NO_x$ activity, due to the existence of the "fast SCR" reaction ($2NH_3 + NO + NO_2 \rightarrow 2N_2 + 3H_2O$). In this study, the concentrations of $NO_2$ production over W/CZ-*T* catalysts are shown in Fig. 2a *via* carrying out the seperated NO oxidation. Although more $NO_2$ was formed over W/CZ-600 than over W/CZ-500 at above 350 °C, the NO conversion for the four catalysts decreased in the order of W/CZ-500 > W/CZ-600 > W/CZ-700 > W/CZ-400 in the low-temperature range, which is in agreement with the increasing sequence of the low-temperature $NH_3$-SCR activity for the four catalysts. This indicated that W/CZ-500 was more efficient than the other catalysts for NO oxidation during the $NH_3$-SCR reaction, so it displayed the highest low-temperature $NO_x$ conversion.

Moreover, the seperated $NH_3$ oxidation tests were also carried out over catalysts and the results are presented in Fig. 2b. W/CZ-400 possessed the highest $NH_3$ oxidation ability among the four catalysts. The activity of $NH_3$ oxidation over the catalysts increased in the sequence of W/CZ-700 < W/CZ-600 < W/CZ-500 < W/CZ-400, which was consistent with the order of the high-temperature $NO_x$ conversion in Fig. 1a. This meant that W/CZ-700 possessed the highest $NH_3$-SCR activity in the high temperature range (above 400 °C), while the minimum high-temperature $NO_x$ conversion was obtained over the W/CZ-400 catalyst. Furthermore, it could be seen that NO was the main product besides $N_2$ for the $NH_3$ oxidation reaction, and no more than 5 ppm $N_2O$ was generated over all catalysts, shown in the insets of Fig. 2b. However, the generated amount of NO over W/CZ-500 was obviously larger than those over W/CZ-600 and W/CZ-700 catalysts, which further proved that the decrease in the high-temperature $NO_x$ conversion of W/CZ-500 can be ascribed to the generation of more NO from the non-selective oxidation of $NH_3$.

**3.1.3 $H_2O$ and $SO_2$ tolerance.** The $H_2O$ and $SO_2$ from the diesel exhaust usually induces a deactivation of the $NH_3$-SCR catalyst in the practical operation conditions; thus, it is significantly to investigate the resistance of the sulphur and water vapour of W/CZ-500 and W/CZ-600 catalysts. As displayed in Fig. 3, the de$NO_x$ activities of W/CZ-500 and 600 catalysts were both affected by injecting 10 vol% $H_2O$ and 100 ppm $SO_2$ into the reaction gas, especially below 275 °C. Table 1 summarizes the related values of $NH_3$-SCR activity over the two catalysts in different reaction conditions. The influence of $SO_2$ was greater than that of $H_2O$ on the SCR activity. The negative effects of $H_2O$ and $SO_2$ resulted from the competitive adsorption between water vapour molecules and ammonia molecules, inhibiting the reaction between $NH_3$ and NO, and the deposited sulphates species cover the active sites on the catalyst surface.[14,15] Moreover, the effects of $H_2O$ and $SO_2$ on the $NO_x$ conversion of W/CZ-600 were smaller than those of the W/CZ-500 catalyst (from Table 1). It could be that more active sites could adsorb more

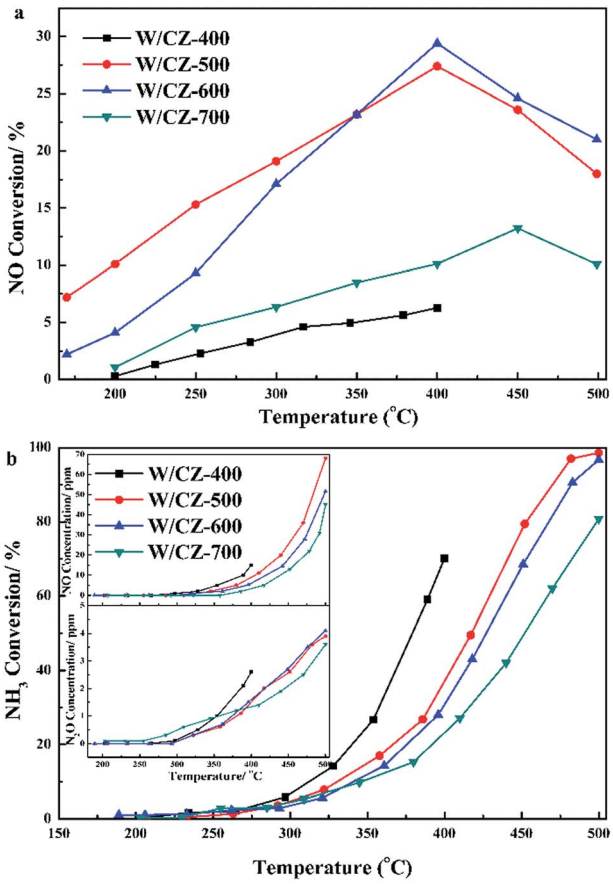


Fig. 2 Separated NO (a) and $NH_3$ (b) oxidation activity over W/CZ-*T* catalysts. Reaction conditions: 500 ppm NO (when used), 500 ppm $NH_3$ (when used), 5% $O_2$, $N_2$ as balance, total flow rate: 1250 mL $min^{-1}$, GHSV: 30 000 $h^{-1}$.

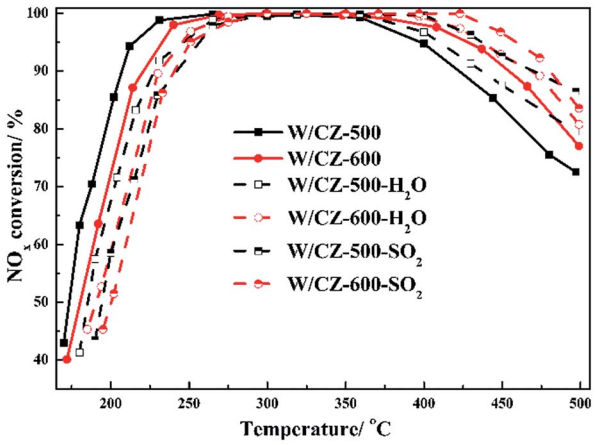


Fig. 3 Effects of $H_2O$ and $SO_2$ on the $NH_3$-SCR activity over W/CZ-500 and W/CZ-600. Reaction conditions: 500 ppm NO, 500 ppm $NH_3$, 5% $O_2$, 10 vol% $H_2O$ (when used), 100 ppm $SO_2$ (when used) and $N_2$ as balance, the total gas rate: 1250 mL $min^{-1}$, GHSV: 30 000 $h^{-1}$.

Table 1 The comparisons of $NH_3$-SCR activity between W/CZ-500 and W/CZ-600 in different reaction conditions

| | W/CZ-500 (°C) | | W/CZ-600 (°C) | |
|---|---|---|---|---|
| Reaction conditions | $T_{50}$ | $T_{90}$ | $T_{50}$ | $T_{90}$ |
| Without | 173 | 205 | 180 | 220 |
| $H_2O$ | 186 | 227 | 190 | 231 |
| $SO_2$ | 194 | 242 | 201 | 240 |

water vapour and sulphur molecules over W/CZ-500 rather than W/CZ-600, because the former catalyst possessed a larger surface area than the latter. It is interesting that the high-temperature (above 360 °C) $NO_x$ conversions over both catalysts were promoted in the presence of $H_2O$ and $SO_2$, respectively, as a result of the increased acidity derived from $H_2O$ and $SO_2$ preventing $NH_3$ non-selective oxidation at a high temperature range.[16,17]

### 3.2 $N_2$ physisorption

Textural properties, including the surface area, average pore radius and cumulative pore volume of W/CZ-*T* catalysts, were listed in Table 2, and the corresponding $N_2$ adsorption–desorption isotherms and pore size distributions of catalysts were shown in Fig. 4a and b, respectively. For all catalysts, the isotherms corresponded to type IV with H2 hysteresis loop, with a relatively wide ink-bottle shaped pore according to the IUPAC classification, indicating the presence of a mesoporous texture.[18–20] With increasing calcination temperature, the $N_2$ adsorbed volume per weight showed an obvious decrease and the closure point of the hysteresis loop also moved to higher $P/P_0$, revealing that much more large mesopores were formed after high temperature calcination of the carrier. The pore radius of the serial catalysts increased as described by Kelvin equation in the following order: W/CZ-700 > W/CZ-600 > W/CZ-500 > W/CZ-400, while the surface area and cumulative pore volume of catalysts exhibited an inverse order as shown in Table 2.

Fig. 4b exhibited the pore size distributions of catalysts with different calcination temperatures of the carrier. For the serial catalysts, as the calcination temperature increased, the pore radii shifted to higher values, which was attributed to the coagulation of nanoparticles, leading to the grain growth and thus to the elimination of smaller pores and the formation of larger ones.[21] It has been proved that the pore radius and pore volume affect the mass and heat transformation of the reactants and products.[22] As summarized in Table 2, W/CZ-400 possessed the largest pore volume, but its pore radius was the smallest among the four samples, and pores were mainly distributed in the range of ≤ 2 nm, from Fig. 4b, which could inhibit the mass transformation of the reactant molecules. W/CZ-700 had the largest pore radius, but most of the pores were collapsed, leading to the decrease in pore volume, which could make the movement of the reactant molecules to the reaction active sits difficult. However, compared with the two catalysts analysed above, the W/CZ-500 and W/CZ-600 catalysts exhibited the appropriate pore volume and radius, which was beneficial to the mass transformation of the reactant molecules and the contact with the active sites, and finally improved the $NH_3$-SCR activity. Moreover, the decreasing ratio (summarized in Table 2) of the

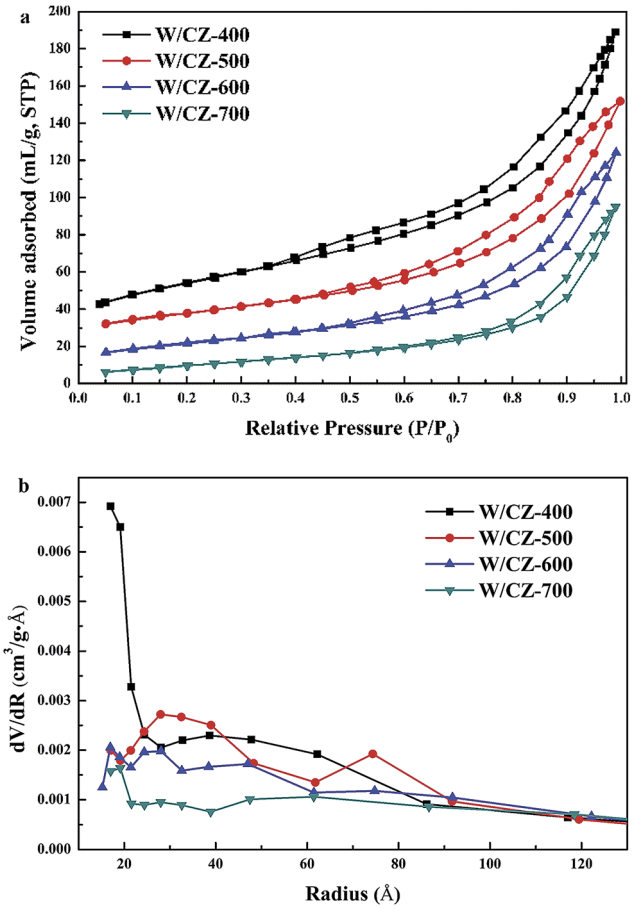


Fig. 4 Nitrogen adsorption/desorption isotherms (a) and the pore size distributions (b) of W/CZ-*T* catalysts.

Table 2 Textural properties of W/CZ-*T* catalysts

| Samples | Surface area ($m^2\ g^{-1}$) | Pore volume ($cm^3\ g^{-1}$) | Pore radius (nm) | Decreasing rate of the surface area (%) |
|---|---|---|---|---|
| W/CZ-400 | 112.0 | 0.24 | 3.9 | — |
| W/CZ-500 | 93.6 | 0.21 | 5.3 | 16.4 |
| W/CZ-600 | 82.9 | 0.19 | 5.7 | 11.4 |
| W/CZ-700 | 52.8 | 0.15 | 6.0 | 33.1 |

surface area from W/CZ-500 to W/CZ-600 was smaller than those from W/CZ-400 to W/CZ-500 and from W/CZ-600 to W/CZ-700. This suggested that the W/CZ-500 and W/CZ-600 catalysts, with the support calcined at the temperature range of 500–600 °C, could hold relatively stable textural properties.

### 3.3 XRD

XRD patterns of W/CZ-*T* catalysts are depicted in Fig. 5 and the detailed parameters were listed in Table 3. Cubic $Ce_{0.75}Zr_{0.25}O_2$ phases (PDF-28-0271) were detected in the XRD patterns of W/CZ-400, W/CZ-500 and W/CZ-600, and with enhancing calcination temperature, an increase in the intensity of diffraction peaks could be seen due to better crystallization of this cubic phase. It was worth noting that the $2\theta$ value showed a slight shift to higher values with increasing calcination temperature, and the cubic $Zr_{0.4}Ce_{0.6}O_2$ phase (PDF-38-1439) was detected over W/CZ-700 catalyst (Fig. 5). According to the literature,[19,21] the radius of $Zr^{4+}$ (0.84 Å) is smaller than that of $Ce^{4+}$ (0.97 Å), and the incorporation of zirconia into the ceria lattice led to the shrinkage of the crystal cells, which induced a shift of $2\theta$ value to higher values. Consequently, the incorporation of more zirconia into the ceria lattice resulted in an increase in the $2\theta$ value after higher temperature calcination. Furthermore, in Table 3, the average crystallite size of $Ce_xZr_{1-x}O_2$ calculated by the Scherrer equation was enhanced from 4.9 nm to 6.8 nm by increasing the calcination temperature from 400 °C to 700 °C, which suggested a progressive increase of Zr content into the Ce cubic lattice and the crystal sintering with the increase of the calcination temperature.[22] However, the crystal size of $Ce_xZr_{1-x}O_2$ increased by 12.2%, from 4.9 nm at 400 °C to 5.5 nm at 500 °C; but it only increased by 5.4% from 5.5 nm to 5.8 nm, implying that the crystal size was basically unchanged when the calcination temperature increased from 500 °C to 600 °C; when the temperature was further increased to 700 °C, the crystal size increased by 17.2% from 5.8 nm to 6.8 nm. The above results further implied that the catalyst could retain a stable structure when the CZ carrier was calcined between 500 °C and 600 °C.

Additionally, two weak diffraction peaks located at 35.2° and 43.5° could be observed in the pattern of W/CZ-400, which could be ascribed to the tragonal Zr-rich phases. The presence of the tetragonal Zr-rich phase implies the structural heterogeneity of W/CZ-400, which could depress $NO_x$ conversion.[23] There was no evidence of the presence of any $ZrO_2$ phases from the other three catalysts within the detection limits of the XRD technique, or the remaining zirconia was mostly in amorphous form and was probably located in grain boundaries.[24] The crystallite size of W/CZ-700 evidently increased after calcination at 700 °C, as a result of the particle aggregation; moreover, the transformation from cubic $Ce_{0.75}Zr_{0.25}O_2$ to cubic $Zr_{0.4}Ce_{0.6}O_2$ phase existed in the process of increased calcination from 400 to 700 °C. The above two phenomena both resulted in the decrease in textural properties of W/CZ-700 (in Table 2) and could go against the dispersion of $WO_3$ on CZ, which finally decreased the $NH_3$-SCR activity of W/CZ-700. It was interesting that no diffraction peak ascribed to crystalline tungsten species could be observed, so it could be assumed that the impregnated tungsten oxides were in a highly dispersed or amorphous state on the surface of CZ.

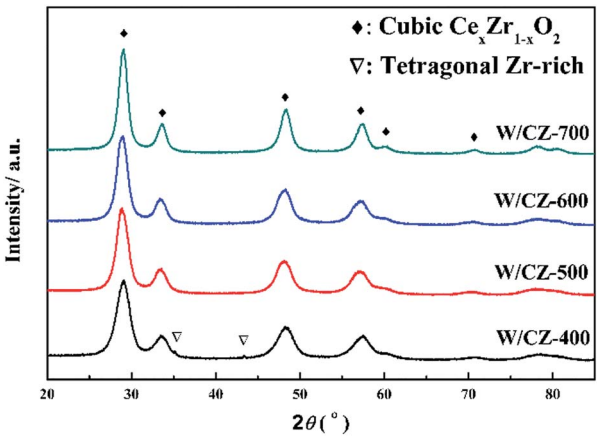


Fig. 5 XRD diffraction patterns collected from W/CZ-*T* catalysts.

Table 3 The detailed parameters of XRD results from W/CZ-*T* catalysts

| Samples | Phase | $2\theta$ (°) | Crystal size (nm) | Increasing rate of the crystal size |
|---|---|---|---|---|
| W/CZ-400 | $Ce_{0.75}Zr_{0.25}O_2$ | 28.75 | 4.9 | — |
| W/CZ-500 | $Ce_{0.75}Zr_{0.25}O_2$ | 28.87 | 5.5 | 12.2% |
| W/CZ-600 | $Ce_{0.75}Zr_{0.25}O_2$ | 28.95 | 5.8 | 5.4% |
| W/CZ-700 | $Zr_{0.4}Ce_{0.6}O_2$ | 29.05 | 6.8 | 17.2% |

### 3.4 Raman spectroscopy

As an effective characterization technique to achieve detailed information about the fine structure, normalized Raman spectroscopy studies were conducted on W/CZ-*T* catalysts, and the results were presented in Fig. 6. The prominent peak at about 465 $cm^{-1}$ corresponded to the $F_{2g}$ vibration mode of cubic $CeO_2$, which could be considered as the symmetric breathing

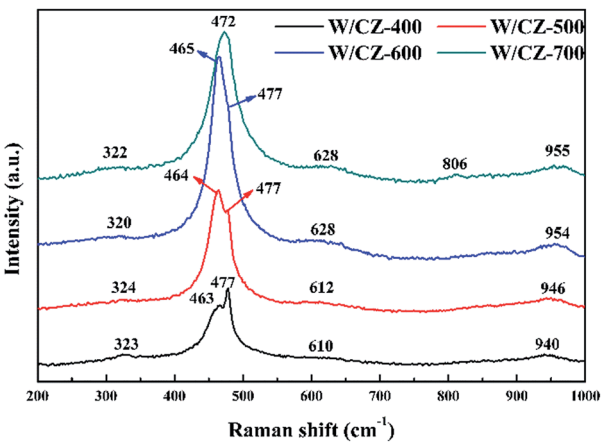


Fig. 6 Raman spectra of W/CZ-500, W/CZ-600 and W/CZ-700 catalysts.

vibrational mode of the O anions around Ce cations.[19,22] However, a shift in the Raman frequency to higher wavenumber from 463 $cm^{-1}$ at 400 °C to 472 $cm^{-1}$ at 700 °C was observed, which resulted from the incorporation of more Zr into the lattice of the cerium zirconium solid solution, as evidenced by XRD results. It was surprise that a less prominent band at around 477 $cm^{-1}$ was visible in the Raman spectra of catalysts; the intensity of this band gradually decreased with increasing the calcination temperature, and finally the band vanished in the spectrum of W/CZ-700. Combined with the analysis of XRD, this Raman band could be ascribed to the tetragonal $ZrO_2$ or Zr-rich phase. The above phenomenon further corroborated the XRD results, which signified that more Zr was incorporated into the Ce–Zr solid solution with the increase of calcination temperature, the composition of the cubic phase was changed and caused the disappearance of the Raman band ascribed to tetragonal $ZrO_2$, until 700 °C.[24] In addition, another two peaks located at around 320 and 620 $cm^{-1}$ for all samples in Fig. 5 could be attributed to the existence of a defective structure.[25]

A broad weak peak centered at approximately 950 $cm^{-1}$ was found for all catalysts, which may be ascribed to the symmetrical W=O stretching mode of the dispersed tungsten oxide species on the surface of the support.[26] The intensity of the band for W/CZ-600 was the strongest among the investigated samples, suggesting that the catalyst possessed more highly dispersed $WO_3$ on the carrier than the other catalysts. Under the same loading conditions of $WO_3$ for the four catalysts, higher surface area was conducive to the dispersion of $WO_3$ on the carrier CZ, while W/CZ-700 with the smallest surface area may result in the micro-crystallization of $WO_3$. In the spectrum, the band at around 806 $cm^{-1}$ was only observed for W/CZ-700, likely due to the presence of polytungstate species, which also showed lower dispersion of $WO_3$ due to smaller surface area after calcination at 700 °C.[27–29] Therefore, higher calcination temperature could inhibit the dispersion of $WO_3$ on the surface of CZ, which may decrease the surface acidity of catalysts and finally affect the $NH_3$-SCR activity.

### 3.5 Acidity

**3.5.1** ***In situ*** **DRIFTS.** To distinguish among the differences in $NH_3$ adsorption behaviours over the catalysts, induced by the calcination temperature of CZ, the *in situ* DRIFTS spectra of $NH_3$ adsorption/desorption were performed in the temperature range of 50–300 °C, and the results were presented in Fig. 7. Fig. 6a showed the $NH_3$ adsorption in the region of 4000–3000 $cm^{-1}$ and 1800–1000 $cm^{-1}$ over W/CZ-*T* catalysts at 100 °C. Several kinds of $NH_3$ species corresponding to different adsorption wavenumbers were observed after the catalysts were exposed to $NH_3$. The bands at 1665 $cm^{-1}$ and 1430 $cm^{-1}$ were assigned to Brønsted acid sites, while the bands at 1030, 1153, 1230, 1325 and 1602 $cm^{-1}$ were attributed to Lewis acid sites.[9] The bands in the range of 3000–3500 $cm^{-1}$ were observed in the spectrum due to contributions from $\nu_{as}$ (N–H), $\nu_s$ (N–H), $2\delta_{as}$ (H–N–H), $2\delta_s$ (H–N–H) and $\delta_{as}$ (H–N–H) modes of ammonia adsorbed on the Lewis acid sites.[30–33] Previous researchers proposed that the increased Lewis acid sites could help to promote the low-temperature $NH_3$-SCR activity, but would lead to the unselective oxidation of $NH_3$ at high temperatures, while more Brønsted acid sites could facilitate $NH_3$ adsorption instead of $NH_3$ oxidation and promote the high-temperature $NH_3$-SCR.[31,34,35] Increasing the calcination temperature of CZ obviously affected the band intensity of $NH_3$ adsorption at 100 °C, as shown in Fig. 7a. The band intensity assigned to Lewis acid sites over W/CZ-500 was the highest among the serial catalysts, but the intensity obviously decreased with further increasing the calcination temperature. However, the band intensity of Brønsted acid sites was gradually improved with increasing the calcination temperature and W/CZ-700 possessed the highest intensity. The changes in the band intensity of DRIFTS were in good accordance with the $NH_3$-SCR activity over W/CZ-*T* catalysts: W/CZ-500 displayed the best low-temperature de$NO_x$ activity, while W/CZ-600 and W/CZ-700 presented higher $NO_x$ conversion at high temperatures.

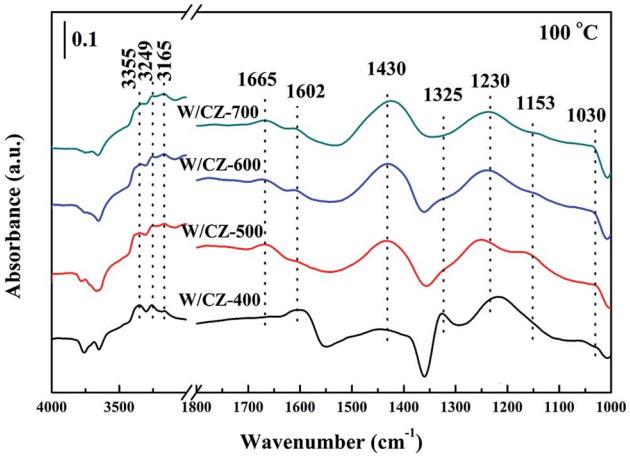


Fig. 7 DRIFTS spectra of $NH_3$ adsorption of W/CZ-*T* catalysts at 100 °C.

In order to further investigate the acid strength, $NH_3$ desorption was performed on the W/CZ-*T* series catalysts in the temperature range of 50–300 °C, and the results were displayed in Fig. 8a–d. For the four catalysts, peak intensities corresponding to both Lewis and Brønsted acid sites decreased with increasing measurement temperature, and the Lewis acid sites presented higher stability, compared with the Brønsted acid sites: at 300 °C, the band at 1240 $cm^{-1}$ could be obviously observed, whereas the band at about 1430 $cm^{-1}$ nearly disappeared, except for W/CZ-700, which could be a reason for the higher activity of W/CZ-700 than other catalysts at high temperatures.

To illustrate in detail the relationships between the changes in acid sites and the $NH_3$-SCR activity, the Lewis and Brønsted acidities of W/CZ-*T* catalysts were obtained by calculating the areas of the corresponding DRIFTS spectra (from Fig. 8a–d) at the different temperatures, and the results were shown in Fig. 7e and f, respectively. The total acidity (Lewis acidity plus Brønsted acidity) of catalysts decreased in the sequence: W/CZ-500 > W/CZ-600 > W/CZ-700 > W/CZ-400. Both Lewis and Brønsted acidities over all catalysts decreased with increasing

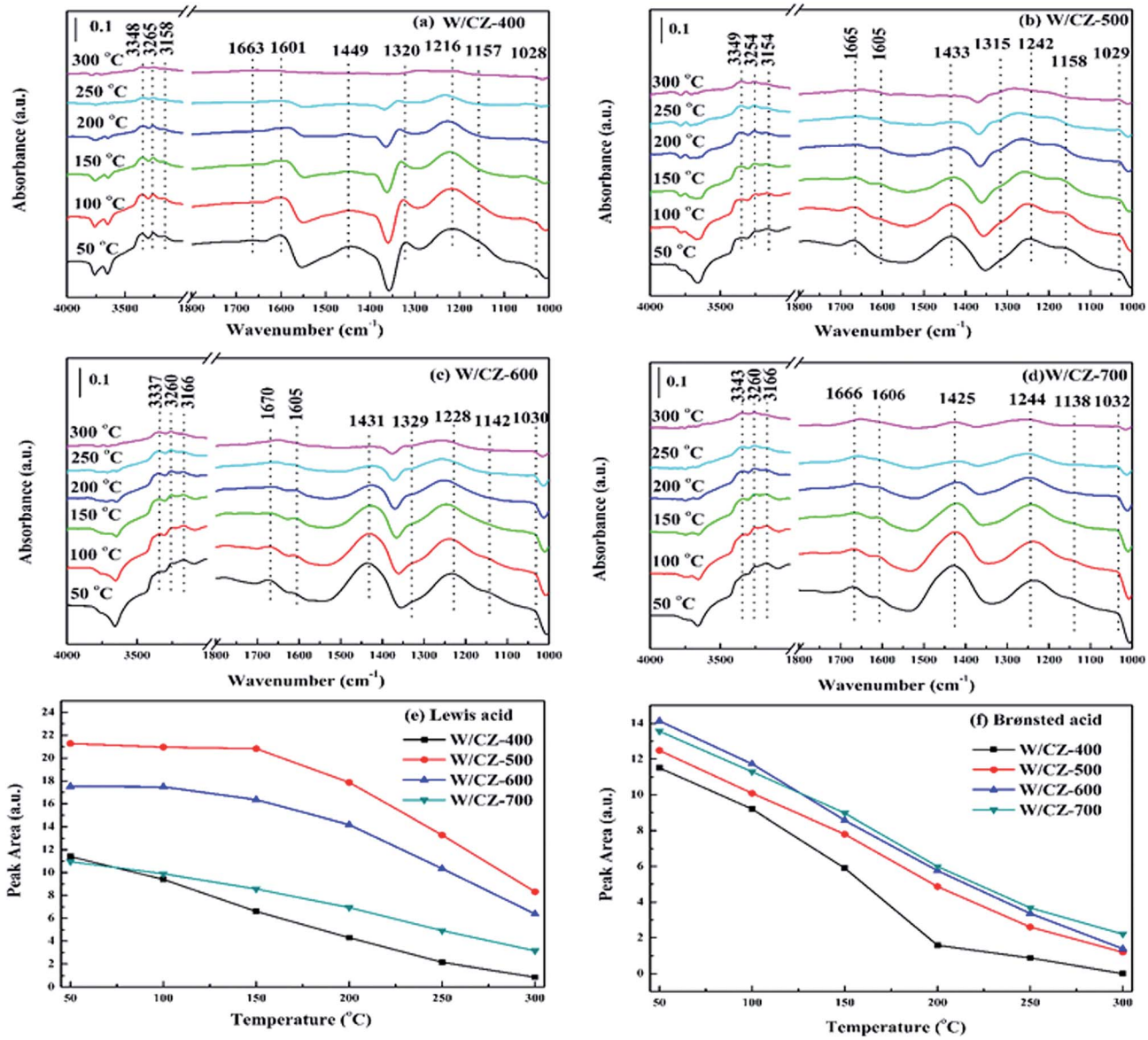


Fig. 8 DRIFTS spectra of $NH_3$ adsorption of (a) W/CZ-400, (b) W/CZ-500, (c) W/CZ-600 and (d) W/CZ-700 in the temperature range of 50–300 °C, and the changes of (e) Lewis and (f) Brønsted acidities with increasing the desorption temperature over W/CZ-*T* catalysts.

measurement temperature. Among the investigated catalysts, W/CZ-500 possessed the largest amount of Lewis acid sites at each temperature. Further improving the calcination temperature resulted in the decline of the total Lewis acidity over W/CZ-600 and W/CZ-700, while the total Lewis acidity of W/CZ-400 was lower than that of W/CZ-700, as shown in Fig. 8e. The above analyses were consistent with the low-temperature SCR activity, because the literature has proposed that a low reaction temperature was favourable for $NH_3$ adsorption to form Lewis acid sites, which was beneficial for improving the low-temperature $NH_3$-SCR activity.[31,34,35] Furthermore, in Fig. 8e, the amount of the total Brønsted acidity was gradually enhanced by improving the calcination temperature of CZ from 400 °C to 700 °C, which meant that the increase in the calcination temperature resulted in the generation of more Brønsted acid sites on the catalyst surface. $NH_3$ oxidation was mostly carried out on the Lewis acid sites rather than on Brønsted acid sites; more Brønsted acid sites could inhibit the oxidation of $NH_3$ and promote the high-temperature $NH_3$-SCR activity.[8,35] The changes in $NH_3$-SCR activity in Fig. 1 and $NH_3$ oxidation activity in Fig. 2b both followed the above rules. In short, W/CZ-500, with the most Lewis acid sites and the relatively small amount of Brønsted acid sites, showed the highest low-temperature SCR activity and relatively lower high-temperature activity; while W/CZ-600 (700) possessed better high-temperature activity than other W/CZ-*T* catalysts.

**3.5.2 $NH_3$-TPD.** The $NH_3$-TPD experiment was employed to estimate the surface acidity of the catalysts with different calcination temperatures of CZ, and the profiles were displayed in Fig. 9. The profiles of all catalysts could be fitted into three

 

overlapping peaks, ascribed to the desorbed $NH_3$ species with different thermal stabilities. The information about acid sites was listed in Table 4, combined with the analysis of *in situ* DRIFTS results. It is clear that the effects on total amount and strength of acid sites were observed as a result of enhancing the calcination temperature of the carrier. From Table 4, the decreased sequence of the total acidities was W/CZ-500 > W/CZ-600 > W/CZ-700 > W/CZ-400, which is in accordance with the results achieved from DRIFTS. The weak Lewis acid sites ($L_1$) were ascribed to the coordinatively unsaturated $Ce^{n+}$ or $Zr^{n+}$ sites, the strong Lewis acid sites ($L_2$) were associated with $W^{n+}$ sites, and the Brønsted acid sites (B) were derived from surface hydroxyl groups.[9,13,36] As listed in Table 4, W/CZ-400 displayed the smallest total acid, the L and B acid amounts both showed rising trends with an increase in the calcination temperature: W/CZ-500 possessed the largest L acid and total acid, W/CZ-600 held more B acid than other catalysts, while W/CZ-700 had a similar amount of B acid and total acid to W/CZ-600. This analysis was basically consistent with the results of *in situ* DRIFTS. The total acid amount of W/CZ-500 was larger than those of W/CZ-600 and 700, because the latter possessed lower surface areas, related to the higher calcination temperatures. In short, the $NH_3$-TPD results also proved that the calcination temperature of CZ remarkably affected the surface acidity of W/CZ-*T* catalyst: among the investigated samples, W/CZ-500 possessed the largest amount of L acid and W/CZ-600 and W/CZ-700 had more B acid. Thus, the former presented the best low-temperature SCR activity, while the latter displayed better $NO_x$ conversion at higher temperatures.

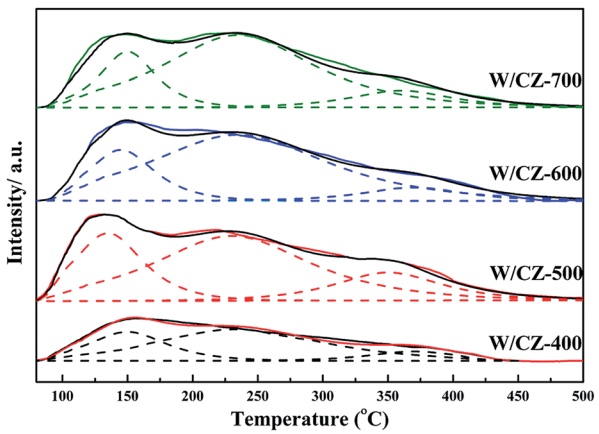


Fig. 9 $NH_3$-TPD profiles of W/CZ-*T* catalysts.

### 3.6 XPS

W/CZ-*T* catalysts were investigated using the XPS technique to achieve a better understanding of the surface chemical state for different elements over the catalysts. The surface atomic concentrations of elements were summarized in Table 5, and the XPS spectra of Ce 3d and O 1s were presented in Fig. 10a and b, respectively.

The intensities of XPS peaks corresponding to Ce 3d clearly decreased with increasing the calcination temperature of CZ, as shown in Fig. 10a. The atomic ratios of $Ce^{3+}/(Ce^{3+} + Ce^{4+})$ in Ce on the catalyst surface were calculated by referring the literature, and the value of W/CZ-500 was obviously larger than those of other catalysts.[8,35] It is well known that more $Ce^{3+}$ could generate the charge imbalance and unsaturated chemical bonds, which could promote the formation of oxygen vacancies and less bound oxygen.[9] The curves of O 1s could be fitted to two peaks for all the catalysts, shown in Fig. 10b. The primary peak centered at about 529.5 eV was attributed to the lattice oxygen $O_2^{2-}$ in metal oxides, denoted as $O_\alpha$, while the additional shoulder peak located at about 531.4 eV was assigned to the chemisorbed oxygen, such as $O_2^-$, $O^-$ and OH groups belonging to some deficiencies in the surface of transition metal oxides and hydroxyl-like groups, labeled as $O_\beta$.[13,37] In Fig. 10b, it was obvious that the binding energy (BEs) of the $O_\alpha$ band for W/CZ-400 was lower than (about 0.5 eV) that of other catalysts, but further increasing the calcination temperature of CZ did not lead to an obvious change in the BE of O 1s. The above phenomena indicated that W/CZ-400 possessed more lattice oxygen species located at lower BE; *i.e.*, other catalysts had more surface chemisorbed oxygen at higher BE. This is in accordance with the change trend of the relative amount of $O_\beta$ listed in Table 5. The relative amount of $O_\beta$ was quantified based on the area of $O_\beta$ divided by the sum of the area of $O_\alpha$ and $O_\beta$, which were 33.7%, 43%, 37.7% and 35.9% over W/CZ-400, W/CZ-500, W/CZ-600 and W/CZ-700, respectively. The above changes in $O_\beta/(O_\alpha + O_\beta)$ over W/CZ-*T* catalysts were accompanied by the same trend for the values of $Ce^{3+}/(Ce^{3+} + Ce^{4+})$, because the formation of more $Ce^{3+}$ could directly increase the relative amount of the chemisorbed oxygen species and promote the oxidation ability of catalysts.[28] Thus, more $Ce^{3+}$ and surface chemisorbed oxygen were helpful to promote the oxidation of NO to $NO_2$, which was

Table 4 The amount of surface acids calculated from $NH_3$-TPD over W/CZ-*T* catalyst

| | Low temperature | | High temperature | | | | |
|---|---|---|---|---|---|---|---|
| Samples | $T^a$ (°C) | $L_1$ (a.u.) | $T^a$ (°C) | B (a.u.) | $T^a$ (°C) | $L_2$ (a.u.) | Total (a.u.) |
| W/CZ-400 | 150 | 2930 | 237 | 6904 | 372 | 961 | 10 795 |
| W/CZ-500 | 134 | 6982 | 229 | 13 507 | 350 | 3830 | 24 319 |
| W/CZ-600 | 146 | 4405 | 236 | 15 263 | 368 | 1550 | 21 218 |
| W/CZ-700 | 151 | 4020 | 234 | 14 960 | 362 | 1973 | 20 953 |

[a] Central temperature of the reduction peak.

Table 5 Surface atom concentration of different elements and other information from XPS of W/CZ-*T* catalysts

| Samples | Surface atom concentration from XPS (%) O | Ce | Zr | W | $O_\beta/(O_\alpha + O_\beta)$ (%) | $Ce^{3+}/(Ce^{3+} + Ce^{4+})$ (%) |
|---|---|---|---|---|---|---|
| W/CZ-400 | 72.9 | 15.1 | 9.4 | 2.6 | 33.7 | 19.5 |
| W/CZ-500 | 78.8 | 11.1 | 7.1 | 3.0 | 43.0 | 22.7 |
| W/CZ-600 | 77.7 | 9.1 | 9.5 | 3.7 | 37.7 | 20.5 |
| W/CZ-700 | 77.6 | 6.4 | 11.4 | 4.6 | 35.9 | 18.6 |

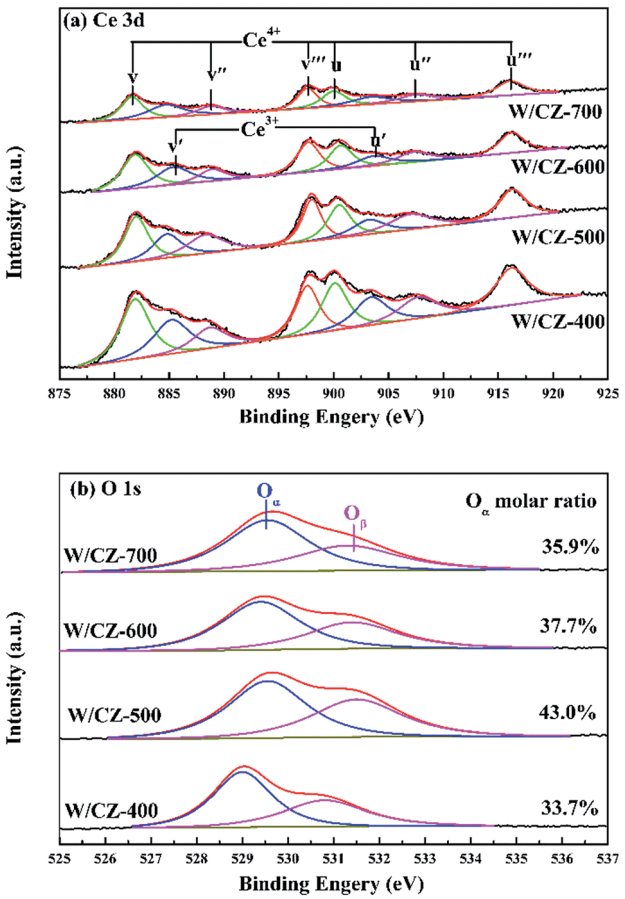


Fig. 10 XPS spectra of W/CZ-*T* catalysts: (a) Ce 3d and (b) O 1s.

well in agreement with the results of NO oxidation (Fig. 2a). It has been proved that the low-temperature $NH_3$-SCR activity can be accelerated by introducing some $NO_2$ into the $NH_3$-SCR system due to the "Fast SCR" reaction.[38] Therefore, W/CZ-500 displayed the best low-temperature $NH_3$-SCR activity because of the largest amounts of $Ce^{3+}$ and surface chemisorbed oxygen among the investigated catalysts.

### 3.7 $H_2$-TPR

Fig. 11 displayed the $H_2$-TPR profiles of W/CZ-*T* catalysts to estimate the effect of the calcination temperature of CZ on the reducibility of different catalysts. $H_2$ consumption of different reduction peaks was calculated by deconvoluting the curves and using CuO as the standard sample, the results were listed in Table 6. As seen from Fig. 11, peak 1 was ascribed to the reduction of the surface active oxygen from CZ mixed oxides; peak 2 could be attributed to the reduction of the lattice oxygen from the bulk metal oxides, *i.e.*, non-active lattice oxygen.[12,39] Obviously, the calcination temperature of the carrier modified the redox properties of W/CZ-*T* catalysts. In Fig. 11, the central temperatures of the reduction peaks gradually shifted to higher temperatures with improving the calcination temperature, but the reduction temperature of active oxygen species (peak 1) on W/CZ-500 was significantly lower than those of other catalysts by 10–40 °C, implying the occurrence of a more facile reduction over W/CZ-500 at lower temperatures. Moreover, W/CZ-500 possessed the largest amount of surface active oxygen species among the investigated catalysts; the sequence for the amount of surface active oxygen species was W/CZ-500 > W/CZ-600 > W/CZ-700 > W/CZ-400. This trend was consistent with the change in surface chemisorbed oxygen as summarized in Table 5 from XPS, so it also correlated well with the results of NO and $NH_3$ oxidation activity as presented in Fig. 2a and b, which further illuminated the reasons for the excellent low-temperature $NH_3$-SCR activity of W/CZ-500 and the better high-temperature $NO_x$ conversion of W/CZ-600 (700).[28,40]

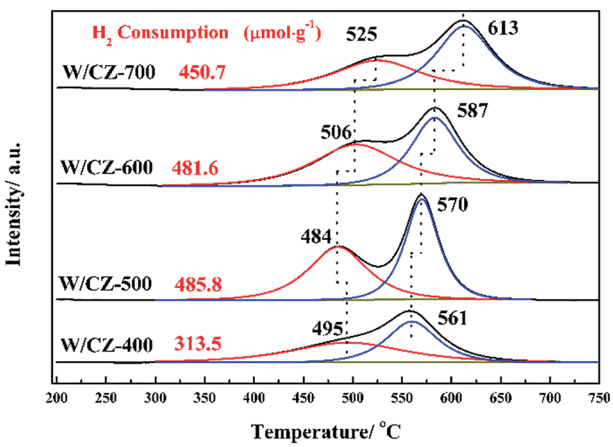


Fig. 11 $H_2$-TPR profiles of W/CZ-*T* catalysts.

Table 6 $H_2$ consumption and central temperature of reduction peaks of W/CZ-*T* catalysts

| Sample | Peak 1 $T_m$[a] (°C) | Peak 1 $H_2$ consumption (μmol $g^{-1}$) | Peak 2 $T_m$ (°C)[a] | Peak 2 $H_2$ consumption (μmol $g^{-1}$) |
|---|---|---|---|---|
| W/CZ-400 | 495 | 163.9 | 561 | 149.6 |
| W/CZ-500 | 484 | 252.3 | 570 | 233.5 |
| W/CZ-600 | 506 | 226.7 | 587 | 254.9 |
| W/CZ-700 | 525 | 187.3 | 613 | 263.4 |

[a] Central temperature of the reduction peak.

 

## 4 Conclusions

$CeZrO_2$ carriers were obtained at different calcination temperatures to prepare $WO_3/Ce_{0.68}Zr_{0.32}O_2$ serial catalysts for application in the $NH_3$-SCR reaction. The calcination temperature remarkably affected the $NH_3$-SCR activity and the operation temperature window of the catalysts. Among them, $WO_3/CeZrO_2$-500 with $CeZrO_2$ calcined at 500 °C showed excellent low-temperature activity (achieved greater than 90% $NO_x$ conversion at 205 °C) and $WO_3/CeZrO_2$-600 exhibited the broadest operation temperature window (220–455 °C). The characterization results demonstrated that the $WO_3/CeZrO_2$-500 catalyst possessed the largest amounts of Lewis acid sites and $Ce^{3+}$ with surface active oxygen species, and the strongest redox properties among all the catalysts, all of which were responsible for its remarkable low-temperature $NH_3$-SCR activity. More Brønsted acid sites were detected over $WO_3/CeZrO_2$-600 than $WO_3/CeZrO_2$-500, which contributed to its having the broadest operation temperature window among the four catalysts. $WO_3/CeZrO_2$ serial catalysts with modest calcination treatment of the carrier are promising candidates for the elimination of $NO_x$ from diesel engines.

## Acknowledgements

This work was financially supported by the National High-Tech Research and Development (863) Program of China (Grant 2015AA034603) and the Science and Technology Project of Chengdu City (Grant 2015-HM01-00475-SF).

## References

1 S. Ding, F. Liu, X. Shi and H. He, *Appl. Catal., B*, 2016, **180**, 766–774.
2 C. Tang, H. Zhang and L. Dong, *Catal. Sci. Technol.*, 2016, **6**, 1248–1264.
3 S. S. R. Putluru, L. Schill, A. Godiksen, R. Poreddy, S. Mossin and R. Fehrmann, *Appl. Catal., B*, 2016, **183**, 282–290.
4 W. Shan, Y. Geng, X. Chen, N. Huang, F. Liu and S. Yang, *Catal. Sci. Technol.*, 2016, **6**, 1195–1200.
5 J. Kašpar, P. Fornasiero and M. Graziani, *Catal. Today*, 1999, **50**, 285–298.
6 H. W. Jen, G. W. Graham, W. Chun, R. W. McCabe, J. P. Cuif, S. E. Deutsch and O. Touret, *Catal. Today*, 1999, **50**, 309–328.
7 Y. Li, H. Cheng, D. Li, Y. Qin, Y. Xie and S. Wang, *Chem. Commun.*, 2008, **12**, 1470–1472.
8 Z. Si, D. Weng, X. Wu, J. Yang and B. Wang, *Catal. Commun.*, 2010, **11**, 1045–1048.
9 Z. Ma, X. Wu, Z. Si, D. Weng, J. Ma and T. Xu, *Appl. Catal., B*, 2015, **179**, 380–394.
10 R. Gao, D. Zhang, P. Maitarad, L. Shi, T. Rungrotmongkol, H. Li, J. Zhang and W. Cao, *J. Phys. Chem. C*, 2013, **117**, 10502–10511.
11 P. Maitarad, D. Zhang, R. Gao, L. Shi, H. Li, L. Huang, T. Rungrotmongkol and J. Zhang, *J. Phys. Chem. C*, 2013, **117**, 9999–10006.
12 H. Xu, Y. Wang, Y. Cao, Z. Fang, T. Lin, M. Gong and Y. Chen, *Chin. Sci. Bull.*, 2014, **59**, 3956–3965.
13 H. Xu, Y. Li, B. Xu, Y. Cao, X. Feng, M. Sun, M. Gong and Y. Chen, *J. Ind. Eng. Chem.*, 2016, **36**, 334–345.
14 Z. Huang, Z. Zhu and Z. Liu, *Appl. Catal., B*, 2002, **39**, 361–368.
15 C. Lin and H. Bai, *Ind. Eng. Chem. Res.*, 2004, **43**, 5983–5988.
16 L. Chen, J. Li, M. Ge and R. Zhu, *Catal. Today*, 2010, **153**, 77–83.
17 H. Xu, Y. Wang, Y. Cao, Z. Fang, T. Lin, M. Gong and Y. Chen, *Chem. Eng. J.*, 2014, **240**, 62–73.
18 D. Zhao, Q. Huo, J. Feng, B. F. Chmelka and G. D. Stucky, *J. Am. Chem. Soc.*, 1998, **120**, 6024–6036.
19 Y. Cui, R. Fang, H. Shang, Z. Shi, M. Gong and Y. Chen, *J. Alloys Compd.*, 2015, **628**, 213–221.
20 G. Leofanti, M. Padovan, G. Tozzola and B. Venturelli, *Catal. Today*, 1998, **41**, 207–219.
21 A. Papavasiliou, A. Tsetsekou, V. Matsouka, M. Konsolakis, I. V. Yentekakis and N. Boukos, *Appl. Catal., B*, 2009, **90**, 162–174.
22 L. Lan, S. Chen, Y. Cao, M. Zhao, M. Gong and Y. Chen, *J. Colloid Interface Sci.*, 2015, **450**, 404–416.
23 P. Ning, Z. Song, H. Li, Q. Zhang, X. Liu, J. Zhang, X. Tang and Z. Huang, *Appl. Surf. Sci.*, 2015, **332**, 130–137.
24 B. M. Reddy and A. Khan, *Langmuir*, 2003, **19**, 3025–3030.
25 B. M. Reddy, A. Khan, P. Lakshmanan, M. Aouine, S. Loridant and J. C. Volta, *J. Phys. Chem. B*, 2005, **109**, 3355–3363.
26 X. Li, M. Shen, H. Zhu, F. Gao, Y. Kong, L. Dong and Y. Chen, *J. Phys. Chem. B*, 2005, **109**, 3949–3955.
27 S. S. Chan, I. E. Wachs and L. L. Murrell, *J. Catal.*, 1984, **90**, 150–155.
28 Y. Peng, K. Li and J. Li, *Appl. Catal., B*, 2013, **140–141**, 483–492.
29 A. Gutiérrez-Alejandre, P. Castillo, J. Ramírez, G. Ramis and G. Busca, *Appl. Catal., A*, 2001, **216**, 181–194.
30 Y. Peng, C. Liu, X. Zhang and J. Li, *Appl. Catal., B*, 2013, **140–141**, 276–282.
31 S. Ding, F. Liu, X. Shi, K. Liu, Z. Lian, L. Xie and H. He, *ACS Appl. Mater. Interfaces*, 2015, **7**, 9497–9506.
32 A. S. Mamede, E. Payen, P. Grange, G. Poncelet, A. Ion, M. Alifanti and V. I. Pârvulescu, *J. Catal.*, 2004, **223**, 1–12.
33 N. Yang, R. Guo, W. Pan, Q. Chen, Q. Wang and C. Lu, *Fuel*, 2016, **169**, 87–92.
34 L. Lietti and P. Forzatti, *J. Catal.*, 1994, **147**, 241–249.
35 H. Xu, Q. Zhang, C. Qiu, T. Lin, M. Gong and Y. Chen, *Chem. Eng. Sci.*, 2012, **76**, 120–128.
36 R. Foo, T. Vazhnova, D. B. Lukyanov, P. Millington, J. Collier, R. Rajaram and S. Golunski, *Appl. Catal., B*, 2015, **162**, 174–179.
37 X. Du, X. Gao, Y. Fu, F. Gao, Z. Luo and K. Cen, *J. Colloid Interface Sci.*, 2012, **368**, 406–412.
38 F. Liu, H. He, Y. Ding and C. Zhang, *Appl. Catal., B*, 2009, **93**, 194–204.
39 J. Yu, Z. Si, L. Chen, X. Wu and D. Weng, *Appl. Catal., B*, 2015, **163**, 223–232.
40 P. W. Seo, S. P. Cho, S. H. Hong and S. C. Hong, *Appl. Catal., A*, 2010, **380**, 21–27.